Anisotropy signature in extended images from reverse-time migration

Paul Sava, Center for Wave Phenomena, Colorado School of Mines
Tariq Alkhalifah, King Abdullah University of Science and Technology

SUMMARY

Reverse-time migration can accurately image complex geologic structures in anisotropic media. Extended images at selected locations in the earth, i.e. at common-image-point gathers (CIPs), carry enough information to characterize the angle-dependent illumination and to provide measurements for migration velocity analysis. Furthermore, inaccurate anisotropy leaves a distinctive signature in CIPs, which can be used to evaluate anisotropy through techniques similar to the ones used in conventional wavefield tomography.

INTRODUCTION

Wave-equation depth migration is powerful and accurate for imaging complex geology, but its potential can only be achieved with high quality models of the earth (Gray et al., 2001). Imaging using reverse-time migration (Baysal et al., 1983; McMechan, 1983), addresses this challenge, although this technique is still fairly computationally intensive, especially in anisotropic media.

Wave-equation imaging of wide-azimuth data (Regone, 2006; Michell et al., 2006; Clarke et al., 2006) is particularly challenging due to the large data volumes and due to the difficulty of interpreting multi-dimensional data. Imaging using extended common-image-point-gathers provides computational savings over alternative methods based on common-image-gathers (Sava and Vasconcelos, 2011). Such efficiency is especially needed in anisotropic media where the cost of imaging is high.

Here we analyze the extended image in anisotropic media, and specifically transversely isotropic (TI) media. These extended images provide image point extensions as a function of space- and time-lags. Embedded in these lag sections is valuable image focusing information, which can be used to analyze the velocity accuracy used in the wavefield extrapolation. As a result, we use such lag sections to characterize the response of the extended images to ignoring anisotropy in RTM. This info, partially decoupling the effects of velocity error from anisotropy error can be used for model building.

THEORY

Conventional wavefield-based imaging consists of two major steps: the wavefield reconstruction and the imaging condition (Berkhout, 1982; Clærbout, 1985). The major driver for the accuracy of this technique are the source and receiver wavefields which depend on space $\mathbf{x} = \{x, y, z\}$ and time t. Wavefield reconstruction in tilted TI anisotropic medium, requires numeric solutions to a pseudo-acoustic wave-equation, e.g. the time-domain method of Fletcher et al. (2009) and Fowler et al. (2010), which consists of solving a system of second-order coupled equations:

$$\frac{\partial^2 p}{\partial t^2} = v_{p_x}^2 H_2[p] + v_{p_z}^2 H_1[q] \ , \quad (1)$$

$$\frac{\partial^2 q}{\partial t^2} = v_{p_n}^2 H_2[q] + v_{p_z}^2 H_1[q] \ . \quad (2)$$

Here, p and q are two wavefields depending on space $\mathbf{x}$ and time t, H_1 and H_2 are differential operators applied to the quantity in the square brackets Alternative formulations, e.g. Duveneck and Bakker (2011) and Zhang et al. (2011) provide expressions for stable extrapolation in more general cases, including TTI. The velocities v_{p_z}, v_{p_x}, and v_{p_n} are the vertical, horizontal and "NMO" velocities used to parametrize a generic TTI medium. If we describe the medium using the parameters introduced by Thomsen (2001), the velocities are related to the anisotropy parameters ϵ and δ by the relations $v_{p_n} = v_{p_z}\sqrt{1+2\delta}$ and $v_{p_x} = v_{p_z}\sqrt{1+2\epsilon}$. Thus, the quantities H_1 and H_2 depend on the medium parameters, as well as θ_a which describes the angle made by the TI symmetry axis with the vertical and ϕ_a the azimuth angle of the plane that contains the tilt.

A conventional imaging condition based on the reconstructed wavefields defines the image as the zero lag of the cross-correlation between the source and receiver wavefields (Clærbout, 1985). An extended imaging condition is a generalization of the conventional imaging condition in that it retains in the output image acquisition or illumination parameters. For example, we can generate image extensions by correlation of the wavefields shifted symmetrically in space (Rickett and Sava, 2002; Sava and Fomel, 2005) or in time (Sava and Fomel, 2006). This separation is simply the lag of the cross-correlation between the source and receiver wavefields (Sava and Vasconcelos, 2011):

$$R(\mathbf{x}, \boldsymbol{\lambda}, \tau) = \sum_{shots} \sum_{t} W_s(\mathbf{x} - \boldsymbol{\lambda}, t - \tau) \, W_r(\mathbf{x} + \boldsymbol{\lambda}, t + \tau) \ . \quad (3)$$

Here R represents the migrated image which depends on position $\mathbf{x}$, and the quantities $\boldsymbol{\lambda}$ and τ are cross-correlation lags in space and time, respectively. The source and receiver wavefields used for imaging, W_s and W_r are the main wavefields indicating by p in equations 1-2. The conventional imaging condition represents a special case of equation 3 for $\boldsymbol{\lambda} = 0$ and $\tau = 0$. Various techniques have been proposed to convert the space- and time-lag extensions into reflection angles (Sava and Fomel, 2003, 2006; Sava and Vlad, 2011;

Sava and Alkhalifah, 2012), thus facilitating amplitude and velocity analysis in complex geologic structures.

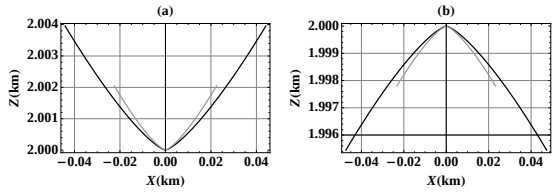

Figure 1: Image point defocusing corresponding to isotropic poststack migration with the correct velocity of 2 km/s in an anisotropic medium with (a) $\eta = 0.1$ (grey curve), $\eta = 0.2$ (black curve), (b) $\eta = -0.1$ (grey curve), and $\eta = -0.2$ (black curve).

Alkhalifah and Fomel (2011) show using anisotropic parameter continuation that the residual anisotropic response for post stack imaging in homogeneous media, and specifically residuals corresponding to the anisotropy parameter η, has a "V"-like shape. This response stems from the fourth-order nature of the η influence on travel-time as a function of offset. A residual reconstruction of such travel-time maps the fourth order influence to a "V" shaped (rather than a residual hyperbolic) moveout as shown in Figure 1. The slope of the "V" depends on the value of η, where negative η provides a flipped "V" signature. We will later see a similar response for the prestack case even in complex media.

In this paper, we show that such a behavior also characterizes the extended images for pre-stack data in complex anisotropic media. This is because the major wavefield complexities are compensated during the wavefield reconstruction in anisotropic media. All that remains are the effects of anisotropy which, for smooth models, resembles the established behavior of poststack depth images. This property could be used to separate the effects of anisotropy from those of velocity, with applications to anisotropic earth model building.

EXAMPLES

The model for our first example, Figure 2(c), consists of a horizontal reflector in a 3D constant velocity model. Figures 2(a)-2(b) depict one snapshot of the wavefields for a source located on the surface in VTI and TTI models, respectively. The models are characterized by the parameters $\epsilon = 0.30$, $\delta = -0.10$ and, for the TTI model, by $\theta_a = 35^\circ$ and $\phi_a = 45^\circ$. Figures 3(a)-3(b) depict extended CIPs at $\{x, y, z\} = \{4, 4, 1\}$ km for many sources distributed uniformly on the surface and correct earth models. All CIPs show focusing at zero lags in space and time, thus indicating wavefield reconstruction with a correct earth model. However, the CIPs constructed with isotropic migration, Figures 3(c) and 3(d), are not focused, thus indicating that the CIPs are sensitive to anisotropy inaccuracy.

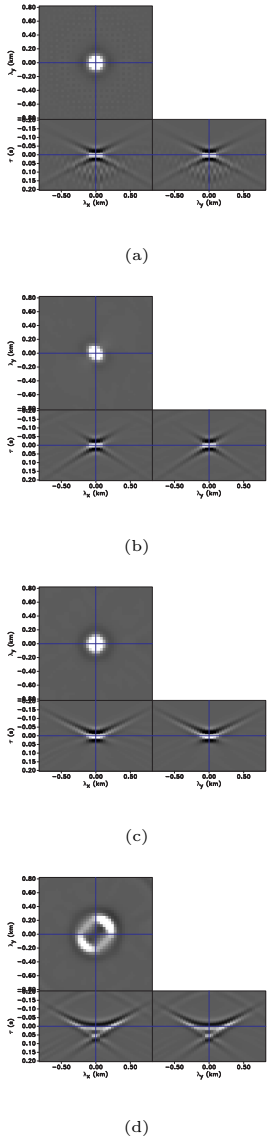

(a)

(b)

(c)

(d)

Figure 3: Extended CIPs at $\{x, y, z\} = \{4, 4, 1\}$ km for many sources distributed uniformly on the surface. The images are obtained by (a)-(b) isotropic migration, and (c)-(d) anisotropic migration of the VTI data (left) and TTI data (right).

The next examples illustrate the behavior of the extended images as a function of anisotropy inaccuracy in constant and laterally heterogeneous models, respectively. The models are shown in Figures 4(a) and 6(a). The data, exemplified in Figures 4(b) and 6(b), are constructed with anisotropy characterized by parameter $\eta = 0.25$. Figures 7(a)-7(c) show the extended images for different shot locations obtained by reverse-time migration with the correct salt model. The figures indicate a dependency of the CIPs with the angle of illumination

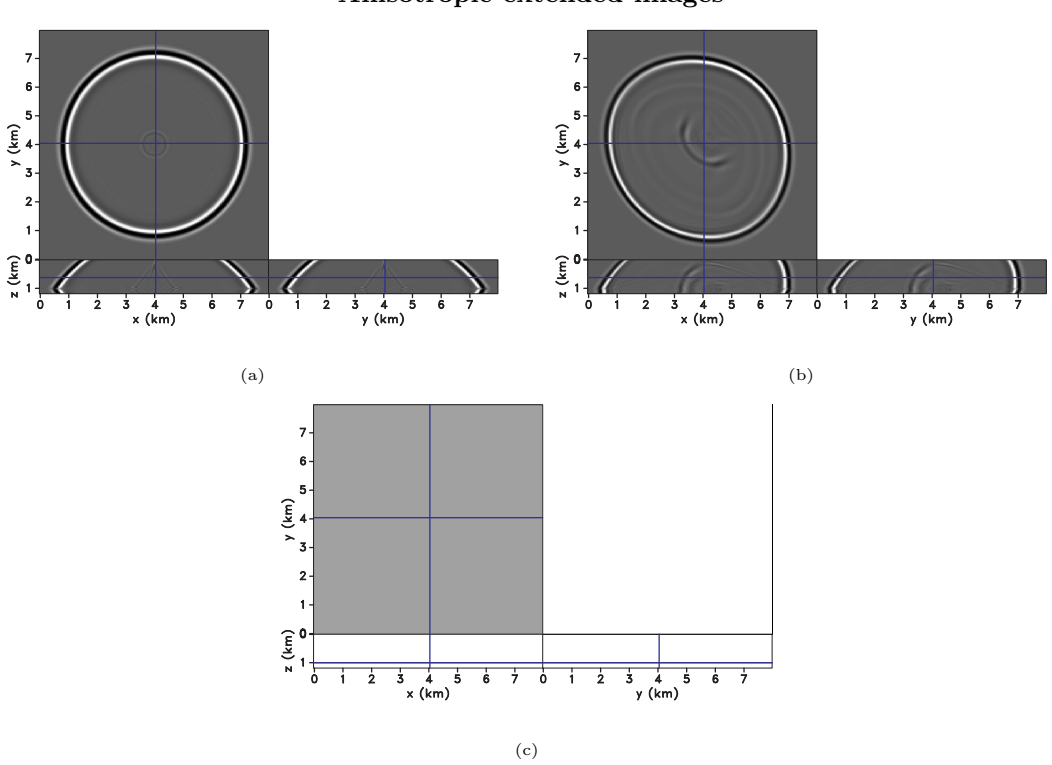

Figure 2: 3D model used to illustrate wide-azimuth extended images in anisotropic media. Panels (a) and (b) show the wavefields corresponding to a single source at $\{x, y\} = \{4, 4\}$ km for VTI and TTI media, respectively. The model (c) consists of a horizontal reflector in constant velocity.

which can be exploited for angle decomposition. The summation for all shots leads to the CIP shown in Figure 7(e) which shows focusing of the image at zero space and time lags. This is due to the fact that all shots leave an imprint on the CIPs at zero space and time lags, but at different slopes which depend on the illumination angle, Figures 7(a)-7(c).

For incorrect η, the resulting response has an overall "V" shape similar to that seen for residual poststack migration. The slope of the "V" flanks, as illustrated in Figures 7(d)-7(f), depend on η. For η close to the correct value, the "V" energy tends to approach the apex, and for correct η it focuses at its apex, Figure 7(e). This general behavior is consistent regardless of the complexity of the medium, especially with respect to the portion of the signature that is near the apex. For comparison, Figures 5(d)-5(e) show extended gathers corresponding to the same values of η as in Figures 7(d)-7(e). Despite the fact that the background velocity model is significantly different, constant vs. salt, the CIPs are comparable, thus indicating that they are mainly influenced by the anisotropy parameters. Of course, for a varying η, such signatures reflect an effective value under the effective medium theory. This property can be exploited for anisotropic migration velocity analysis.

CONCLUSIONS

The distinct anisotropic signatures, needed for parameter estimation, tend to get lost in the mist of the complexity of the velocity in the medium. Extended images preserve such signatures, which allows for direct anisotropy analysis. The slope of the residual moveout in extended CIPs mainly depends on η, which simplifies parameter estimation in anisotropic media. A comparison of extended images between simple and complex models supports our assertion.

ACKNOWLEDGMENTS

This work was supported by the sponsors of the Center for Wave Phenomena at Colorado School of Mines. The authors also thank KAUST for financial support. The reproducible numeric examples in this paper use the Madagascar open-source software package freely available from http://www.reproducibility.org. This research was supported in part by the Golden Energy Computing Organization at the Colorado School of Mines using resources acquired with financial assistance from the National Science Foundation and the National Renewable Energy Laboratory.

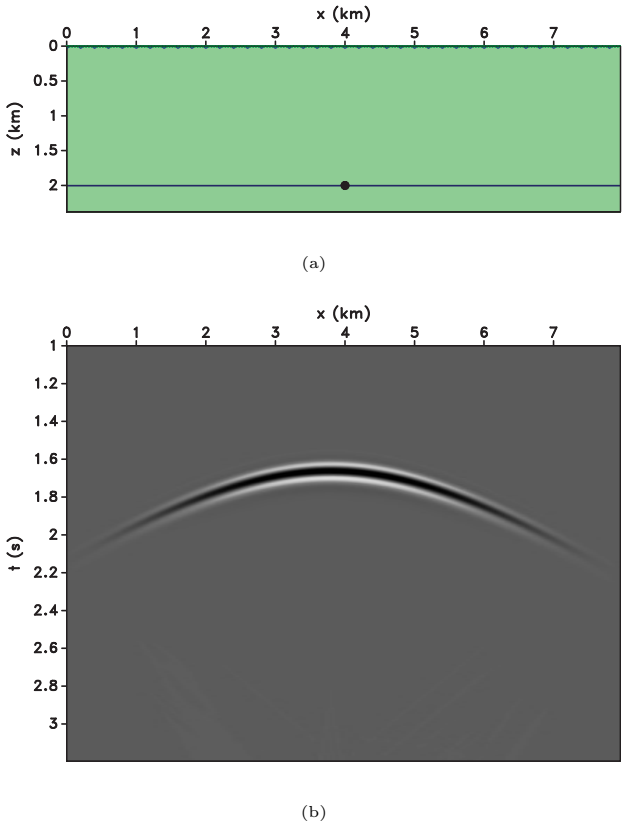

(a) (b)

Figure 4: (a) 2D **constant model** used to study the dependence of the extended CIPs with anisotropy, and (b) one shot gather for a source located at $\{x, z\} = \{3.4, 0\}$ km. The earth model is anisotropic and characterized by parameter $\eta = 0.25$.

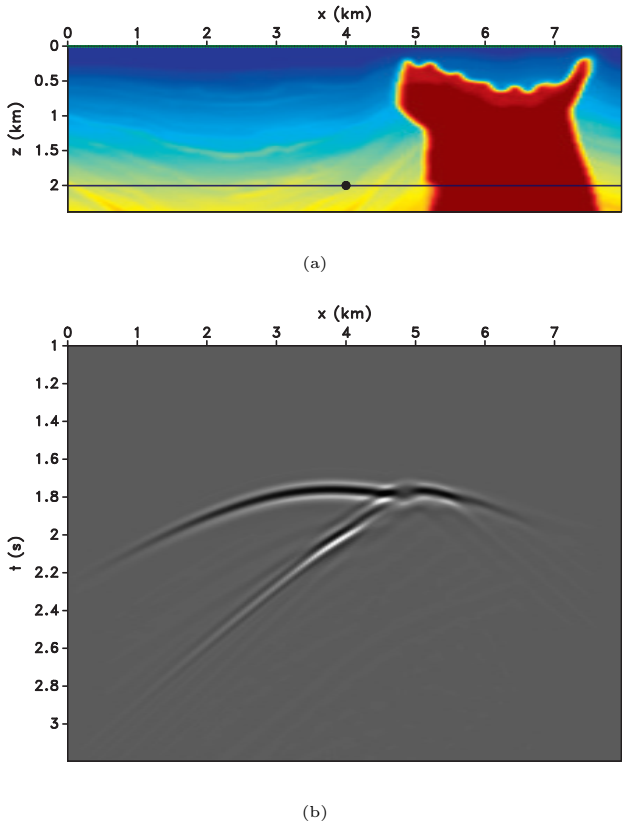

(a) (b)

Figure 6: (a) 2D **salt model** used to study the dependence of the extended CIPs with anisotropy, and (b) one shot gather for a source located at $\{x, z\} = \{3.4, 0\}$ km. The earth model is anisotropic and characterized by parameter $\eta = 0.25$.

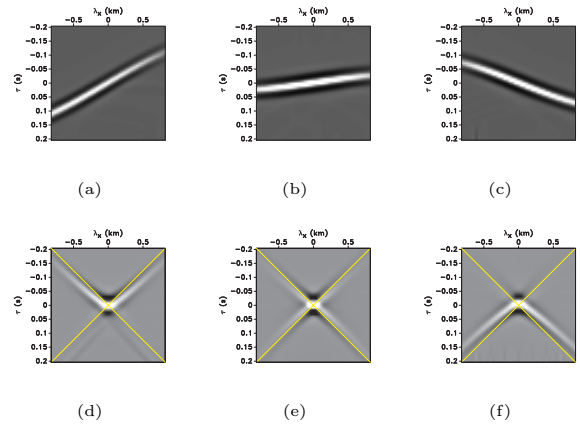

(a) (b) (c) (d) (e) (f)

Figure 5: 2D extended CIPs at $\{x, z\} = \{4, 0\}$ km for the **constant model**, Figure 6(a). The extended images (a)-(c) correspond to individual shots at surface coordinates $x = \{3.2, 4.0, 4.8\}$ km and are obtained from wavefields reconstructed with the correct $\eta = 0.25$. The extended images (d)-(f) correspond to anisotropy characterized by parameter $\eta = \{0.15, 0.25, 0.35\}$.

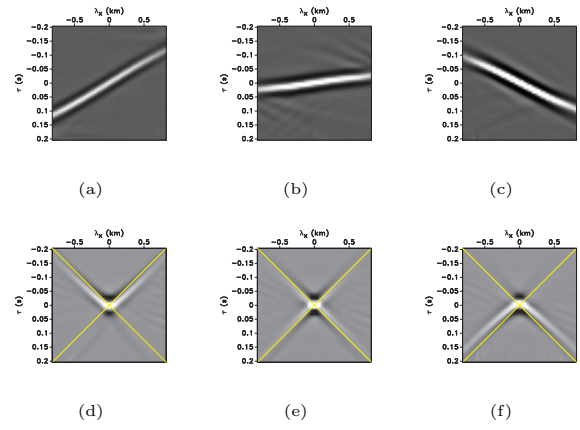

(a) (b) (c) (d) (e) (f)

Figure 7: 2D extended CIPs at $\{x, z\} = \{4, 0\}$ km for the **salt model**, Figure 6(a). The extended images (a)-(c) correspond to individual shots at surface coordinates $x = \{3.2, 4.0, 4.8\}$ km and are obtained from wavefields reconstructed with the correct $\eta = 0.25$. The extended images (d)-(f) correspond to anisotropy characterized by parameter $\eta = \{0.15, 0.25, 0.35\}$.

REFERENCES

Alkhalifah, T., and S. Fomel, 2011, The basic components of residual migration in vti media using anisotropy continuation: J Petrol Explor Prod Technol, **1**, 17–22.

Baysal, E., D. D. Kosloff, and J. W. C. Sherwood, 1983, Reverse time migration: Geophysics, **48**, 1514–1524.

Berkhout, A. J., 1982, Imaging of acoustic energy by wave field extrapolation: Elsevier.

Clærbout, J. F., 1985, Imaging the Earth's interior: Blackwell Scientific Publications.

Clarke, R., G. Xia, N. Kabir, L. Sirgue, and S. Michell, 2006, Case study: A large 3D wide azimuth ocean bottom node survey in deepwater gom: SEG Technical Program Expanded Abstracts, **25**, 1128–1132.

Duveneck, E., and P. M. Bakker, 2011, Stable p-wave modeling for reverse-time migration in tilted ti media: Geophysics, **76**, S65–S75.

Fletcher, R. P., X. Du, and P. J. Fowler, 2009, Reverse time migration in tilted transversely isotropic (TTI) media: Geophysics, **74**, WCA179–WCA187.

Fowler, P. J., X. Du, and R. P. Fletcher, 2010, Coupled equations for reverse time migration in transversely isotropic media: Geophysics, **75**, S11–S22.

Gray, S. H., J. Etgen, J. Dellinger, and D. Whitmore, 2001, Seismic migration problems and solutions: Geophysics, **66**, 1622–1640.

McMechan, G. A., 1983, Migration by extrapolation of time-dependent boundary values: Geophys. Prosp., **31**, 413–420.

Michell, S., E. Shoshitaishvili, D. Chergotis, J. Sharp, and J. Etgen, 2006, Wide azimuth streamer imaging of mad dog; have we solved the subsalt imaging problem?: SEG Technical Program Expanded Abstracts, **25**, 2905–2909.

Regone, C., 2006, Using 3D finite-difference modeling to design wide azimuth surveys for improved subsalt imaging: SEG Technical Program Expanded Abstracts, **25**, 2896–2900.

Rickett, J., and P. Sava, 2002, Offset and angle-domain common image-point gathers for shot-profile migration: Geophysics, **67**, 883–889.

Sava, P., and T. Alkhalifah, 2012, Wide-azimuth angle gathers for anisotropic wave-equation migration: Geophysical Prospecting, in press.

Sava, P., and S. Fomel, 2003, Angle-domain common image gathers by wavefield continuation methods: Geophysics, **68**, 1065–1074.

———, 2005, Coordinate-independent angle-gathers for wave equation migration: 75th Annual International Meeting, SEG, Expanded Abstracts, 2052–2055.

———, 2006, Time-shift imaging condition in seismic migration: Geophysics, **71**, S209–S217.

Sava, P., and I. Vasconcelos, 2011, Extended imaging condition for wave-equation migration: Geophysical Prospecting, **59**, 35–55.

Sava, P., and I. Vlad, 2011, Wide-azimuth angle gathers for wave-equation migration: Geophysics, **76**, S131–S141.

Thomsen, L., 2001, Seismic anisotropy: Geophysics, **66**, 40–41.

Zhang, Y., H. Zhang, and G. Zhang, 2011, A stable tti reverse time migration and its implementation: Geophysics, **76**, WA3–WA11.